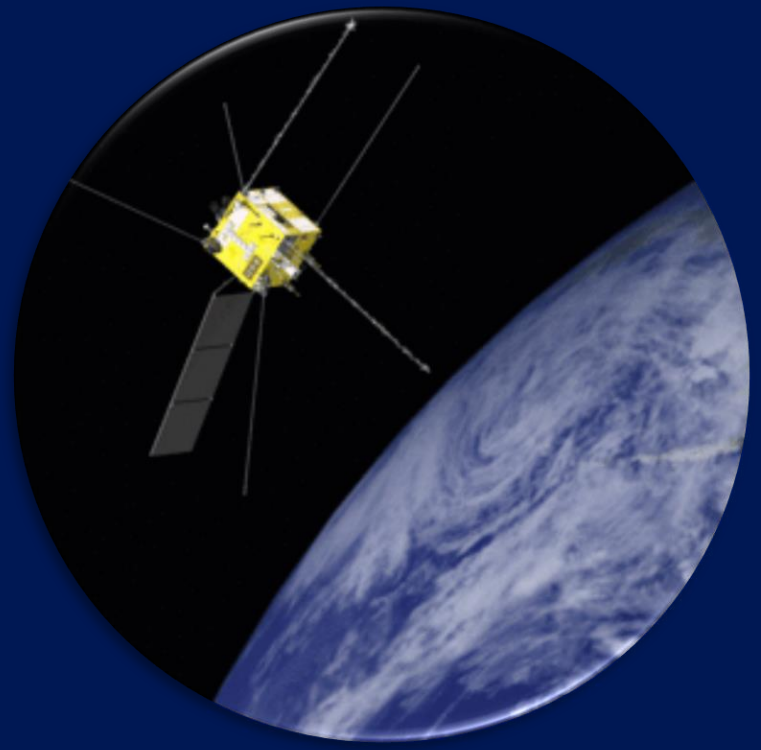

TWEPP 2023

Real-time Signal Processing and Data Acquisition for the Electric Field Detector (EFD-02) on the CSES-02 satellite

Gianmaria Rebustini (INFN)

On behalf of the CSES-Limadou Collaboration

Istituto Nazionale di Fisica Nucleare

Agenzia Spaziale Italiana

Università di Trento

Tor Vergata Università degli Studi di Roma

Università degli Studi di Torino

Outline

- Introduction to the CSES mission, payloads and goals
- General overview: early observations, previous missions and scientific models
- Electric Field Detector (EFD)
- EFD-02: essential components and novelties
- DPU architecture
- Filters and FFT architecture
- Statistical functions block and implementation
- Integer vs custom float arithmetics
- EFD System Verification
- Conclusions

Mission overview

The **China Seismo-Electromagnetic Satellite** (CSES) mission is Chinese-Italian multi-instrumental scientific space program which aims at studying space environment around the Earth

Solar-terrestrial interactions and **solar physics phenomena** (Coronal Mass Ejections or CMEs, solar flares and cosmic ray solar modulation).

To find possible correlations (spatial and temporal) between the **occurrence of seismic events** and…

Observation of **iono-magnetospheric perturbations**

Plasma perturbations

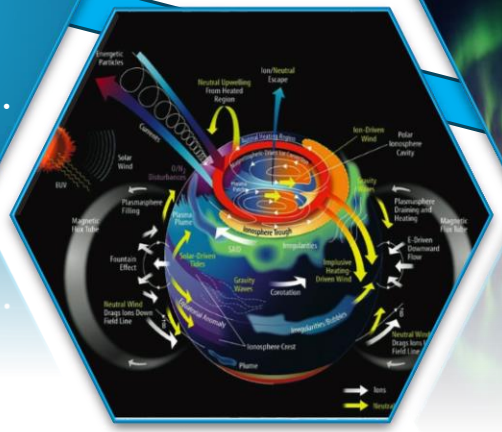

Precipitation of particles from the inner Van Allen belts.

Payloads and observational targets

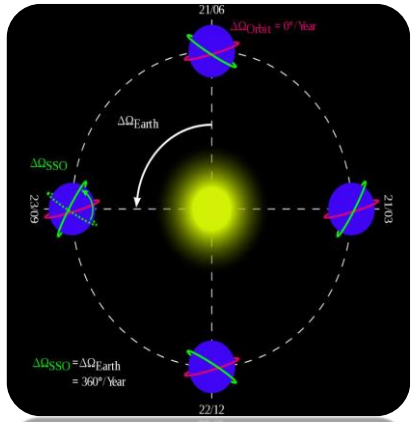

The second satellite of the CSES mission (CSES-02) is expected to be launched in 2024, with an **expected lifetime of 6 years,** after injection in the same sun-synchronous low Earth orbit (LEO, $\sim 500\,Km$ altitude, inclination of $\sim$**98°**.) with a phase shift of 180° with respect to the first satellite.

This second satellite, is meant for optimization of the temporal overlap with the first satellite, and improvement of data quality.

A great advantage is that we have **10** dedicated **instruments on board!**

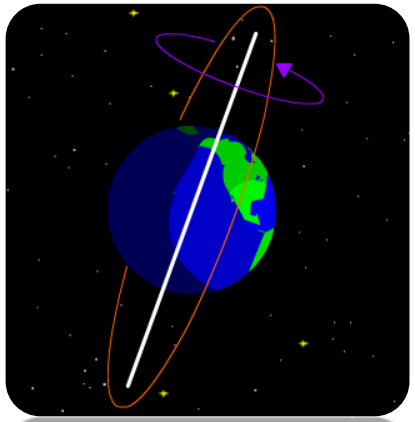

Payloads on board CSES-02:

- **High-Energy Particle Detector (HEPD-02)** and **Medium Energy Electron Detector** to measure particle flux and energy spectrum.
- **Search-Coil Magnetometer (SCM)** and a **High Precision Magnetometer (HPM)** to measure the components and the total intensity of the magnetic field.
- **Electric Field Detector (EFD-02)** to measure the electric field.
- **Plasma analyzer** and **Langmuir probe** to measure the disturbance of plasma in ionosphere.
- **GNSS Occultation Receiver** and a **Tri-Band Beacon** to measure the density of electrons.
- **Ionospheric Photometer.**

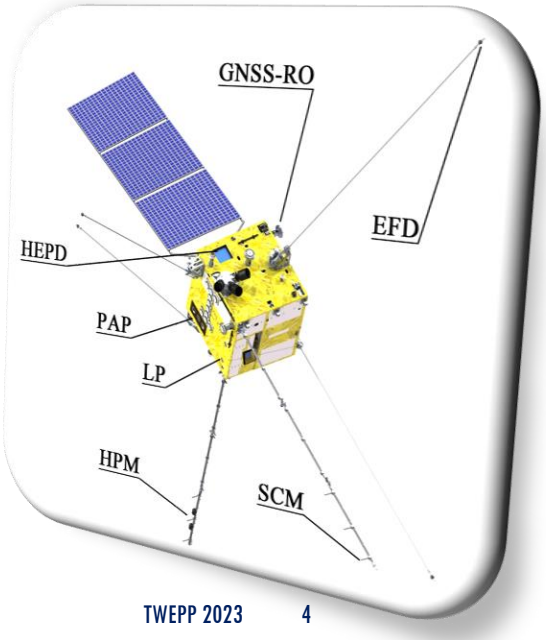

Early observations and previous studies

SEISMIC-RELATED PHENOMENA

- Early Observations from mission non-dedicated to seismic studies
- Radon coupling mechanism
- Ionospheric Disturbances
- Acoustic Gravity Waves
- Electromagnetic Field Measurements
- Particle Precipitation from Van Allen Belts
- Thermal Anomalies
- Remote Sensing and Multi-Parametric Approach

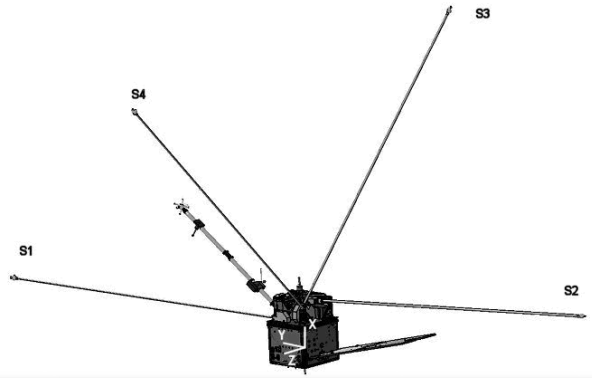

June 29, 2004

DEMETER SATELLITE OBSERVATIONS

- Variability of electromagnetic precursors.
- Relation between ground and space information.
- Correlation between earthquake magnitude, depth and amplitude of possible precursors.
- Extent of the spatial scale of the precursors.
- Temporal advance and clustering of anomalous observations.

Some physical models

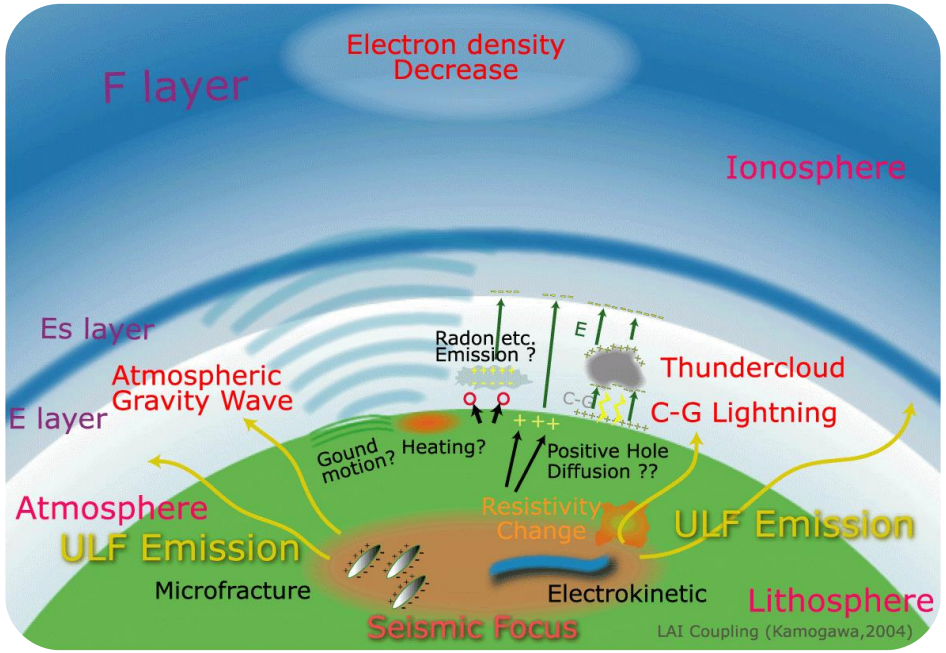

LITHOSPHERE - ATMOSPHERE - IONOSPHERE COUPLING (LAIC) MODEL

EM processes seems to be related to deformation and breaking of rocks that generate earthquakes.

Electromagnetic emissions have been observed during laboratory experiments on rock samples subjected to strong pressures near the moment of rupture of the materials.

Observations of EM disturbances, gas emissions (radon) and thermal perturbations observed by ground monitoring networks in relation to seismic events, especially of great magnitude.

The development of low-altitude satellites for Earth observation has made it possible to study these phenomena from space by monitoring various parameters over large areas of the planet.

Observations:

- EM emissions
- Anomalies in ionospheric and atmospheric parameters (plasma density and Total Electron Content)
- Disturbances in VLF transmissions
- Anomalous flows of precipitating particles from the Van Allen belts

Limits

The intensity of the presumed seismic precursors appears rather difficult to distinguish from the prevailing effects induced by sources external to the geomagnetic cavity and by atmospheric events.

Moreover, the Sun plays a key role in controlling the dynamics of the upper ionosphere which generates (regular and irregular) variations of the ionosphere and magnetosphere following impulsive events such as coronal mass ejections and solar flares - as well as the tropospheric activity.

Some physical models

MAGNETOSPHERIC – IONOSPHERIC – LITHOSPHERIC COUPLING (MILC) MODEL

The basic coupling is hypothesized as being through the Atmospheric Gravity Waves (AGW) and Acoustic Waves (AW).

Such oscillations, developing around the EE (Earthquake Epicentre), perturb the atmosphere in terms of changes in temperature, pressure, ground motion, etc. AGWs can propagate upward and, thus, can drive disturbances in the ionosphere.

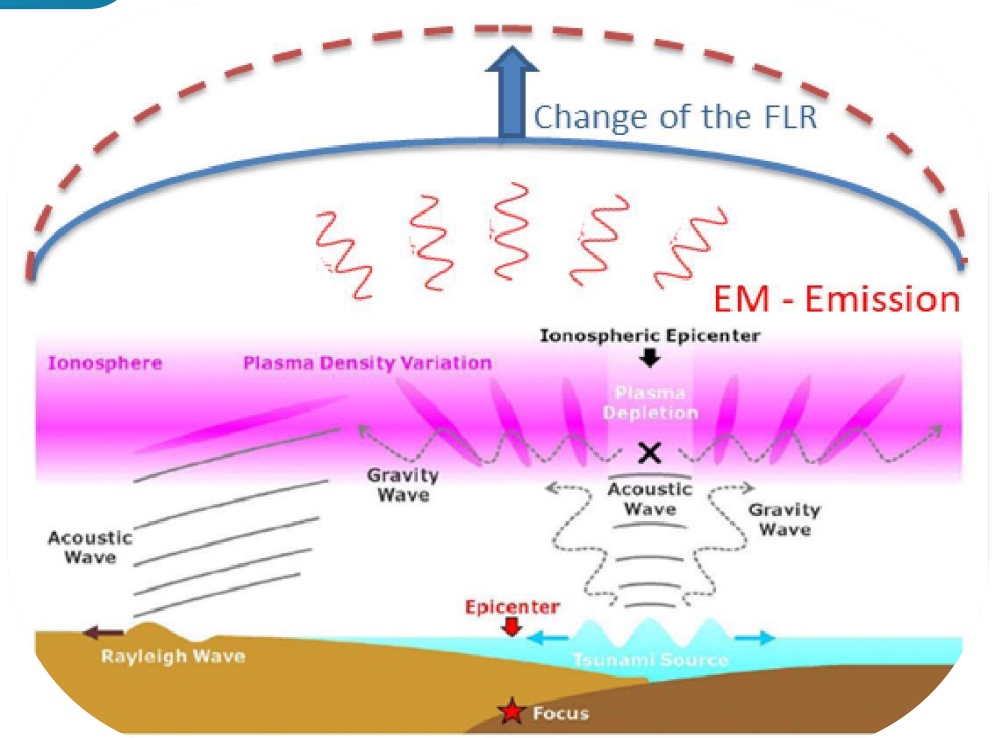

Three causal steps:

An AGW is generated around the EE, propagating through the atmosphere

The AGW interacts mechanically with the ionosphere, creating a local instability in the plasma distribution through a **pressure gradient**.

Such plasma variation put the ionosphere into a "meta-stable" state, giving rise, in the E-layer, to a local non-stationary electric current. This, in turn, generates an **EM wave**

The interaction of such EM waves with the magnetospheric field causes a change in the resonance frequency of the field line, these waves propagate radially with respect to the EE

Electric Field Detector (EFD)

The EFD measures the **differences in electric potential between different pairs of sensors,** called Electric Field Probes (EFPs), installed at the tips of four booms deployed at about 4 m from the satellite.

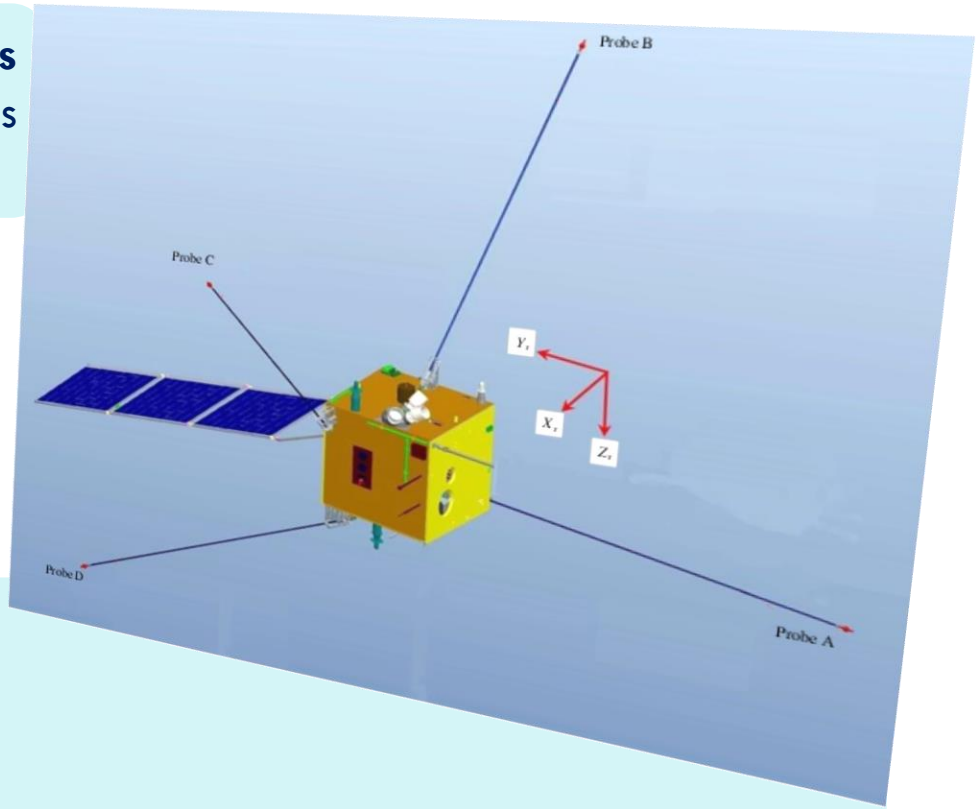

Each of the three Electric field components is obtained as the difference between two probes voltages divided by their relative distance (8.3 m on average), $d_{1,2}$:

$$E_{1,2} = \frac{V_1 - V_2}{d_{1,2}}$$

Thus, EFD is intended to measure:

- **Electric field variations.**
- **Plasma density depletions.**
- **Electromagnetic signals from natural and artificial sources** (e.g., Schumann resonance and VLF antennas).

- Frequencies from 0 to 3.5 MHz
- High Electric Field sensitivity about 1 $\mu V/m$ in the Ultra-Low Frequency (ULF) band.

The Electric Field Detector (EFD-02) is developed by the Italian CSES-Limadou Collaboration. The boom harness (C-Harness) is developed by a Chinese institute, the Lanzhou Institute of Physics.
The measurements carried out by the EFD are considered essential for the entire mission, as they will allow, in association with the magnetic field data, the monitoring of EM waves along the orbit.

EFD-02: essential components

EFD-02 main parts:

1. **The Electric Field Probes (EFPs):** four identical sensors, each of which is housed inside a spherical shell placed at the end of a satellite boom and has the task of detecting the potential with high precision. **A voltage adapter with a high input impedance** is the core of the sensor's Front-End electronics.

2. **The five electronic boards,** placed inside a metal rack (the box in figure) at a specific position:
   - **The Low Voltage Power Supply and Control** (LVPS & CTRL): power supply, housekeeping and TM / TC interface towards the satellite;
   - **The Analog Processing Unit** (APU): analog signal processing board (first filtering and ADC conversion);
   - **The Digital Processing Unit** (DPU): digital processing board, On-Board Data Handling (OBDH), command and control of the payload; described in more detail later.
   - **The SPLITTER** performs the redundancy function of making the HOT or COLD sections operate in case of failure.
   - **The Backplane** for interconnection between electronic boards.

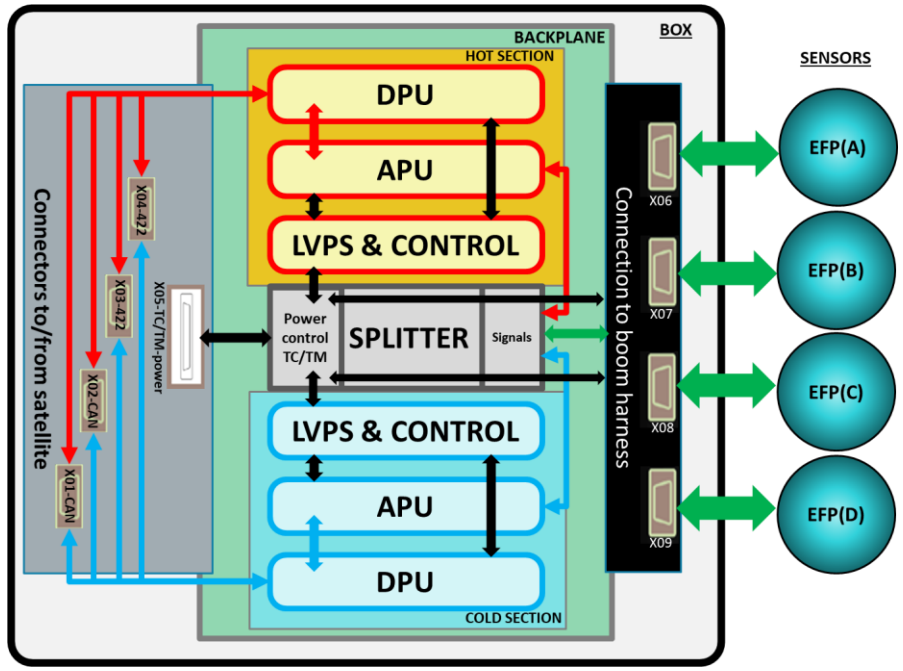

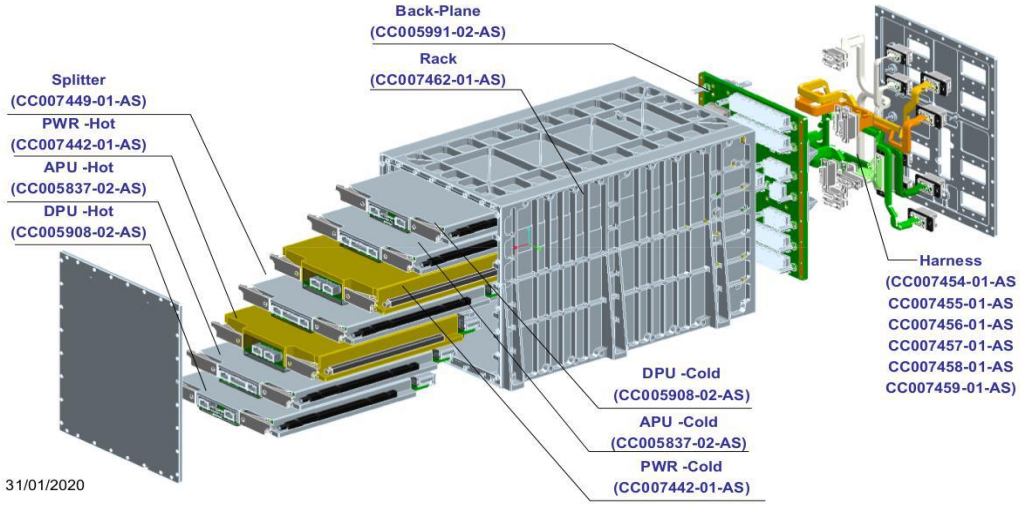

EFD-02: what's new?

Compared to the previous detectors, employed for the same purpose, (EFD-01, ICE) on board CSES-01 and DEMETER missions respectively, EFD-02 has:

1. A **more organized subdivision** of acquired signals into **5 bands** (ULF, ELF, VLF, VLFe, HF).
2. An increased **number of channels** (both for scientific purposes and for redundancy).
3. **Improved bit depth and frequency resolution** (clearest signals and to optimize the S/N ratio).
4. The **possibility to select,** via remote controls from Earth**, the pair of probes for calculating the 3 components of the electric field** (via a matrix of switches).
5. The ability to power off and isolate any of the probes, for both testing purposes and in case of malfunction.
6. A **new bias current control algorithm,** to prevent saturation phenomena in perturbed plasma conditions.

All the choices represent a **trade-off between achieving "high performance"** enabled by advanced electronic technologies and complying with the satellite **spacecraft's limitations** in terms of **power consumption and downlink data rate.**

EFD-02: what's new?

Band	Type	Frequencies band	#channels	Sampling Frequency	Resolution (bit)
ULF	Wave	0 – 100 Hz	4	244 Hz	24
ELF	Wave	19 Hz – 2 kHz	3	4000 Hz	20
VLF	Wave+FFT	1 kHz – 30 kHz	3	60 kHz	16
VLFe	Wave+FFT	21 kHz – 100 kHz	3	200 kHz	16
HF	FFT	21 kHz – 3.5 MHz	3	8 MHz	12

At the high frequencies (**HF** band), the instrument sequentially monitors one of the three electric fields components (x, y, z) at a time with a high switching speed, a mode necessary to meet the budget constraints of consumed power.

The **widening** (w.r.t. Demeter) **of the ULF and VLF bands** (by also including the new VLFe band) **allow improving quality of data** (bit and frequency resolution) **and optimizing data-rate**.

The FFT will be provided as average values (on 50 FFTs), with the relative SD and Kurtosis. In the Burst Mode (Survey + VLF WF + VLFe WF for 2h/d) the total data weight is 82 Gbit/day.

Digital Processing Unit (DPU)

The DPU is based on Zynq xc7z7045 **system on chip** (SOC) from **Xilinx.**

For each ADC there is an interface that performs the functions of: **configuring, controlling** and **input data buffering.**
The acquired data are processed into the FPGA DSP section of the SOC and **stored in Scientific data memory.**
The entire system is controlled by the SOC ARM processor.
The processor has the task of **managing the communication links** (CANBUS and RS422) to / from the satellite, monitoring the health status of the EFD and managing the operating modes of the detector.

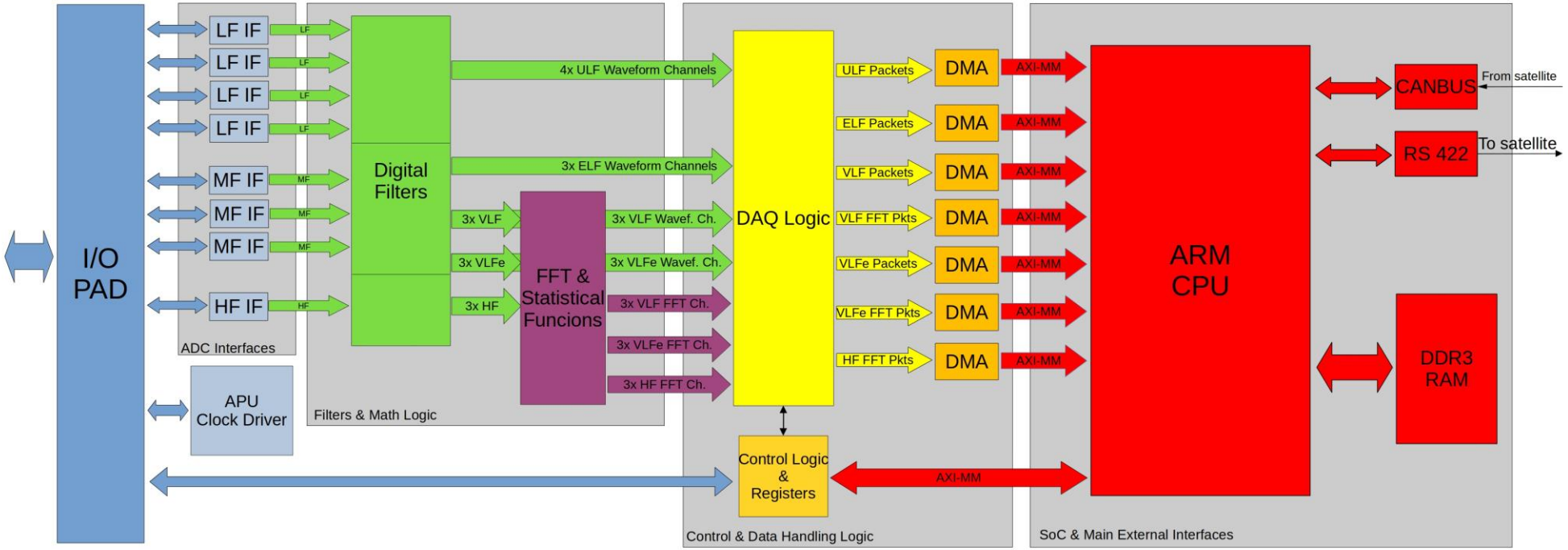

Filters and FFT architecture

-Band division is performed by applying cascading FIR filters on the incoming data channels:

- ULF is derived from Low Frequency channels
- ELF, VLF and VLFe are derived from Medium Frequency channels
- HF is derived from the High Frequency channel, which is hardware multiplexed among the 3 components

-Filters perform also data rate reduction and bit width reduction.

-2048-samples FFTs are calculated with 16bit fixed point arithmetic:

- Hanning windowing
- Radix-2 Lite, Burst I/O or Streaming I/O architecture
- $\frac{2}{N}\sqrt{(re^2 + im^2)}$ amplitude calculation

-FFTs sequences are used for complex statistical observables.

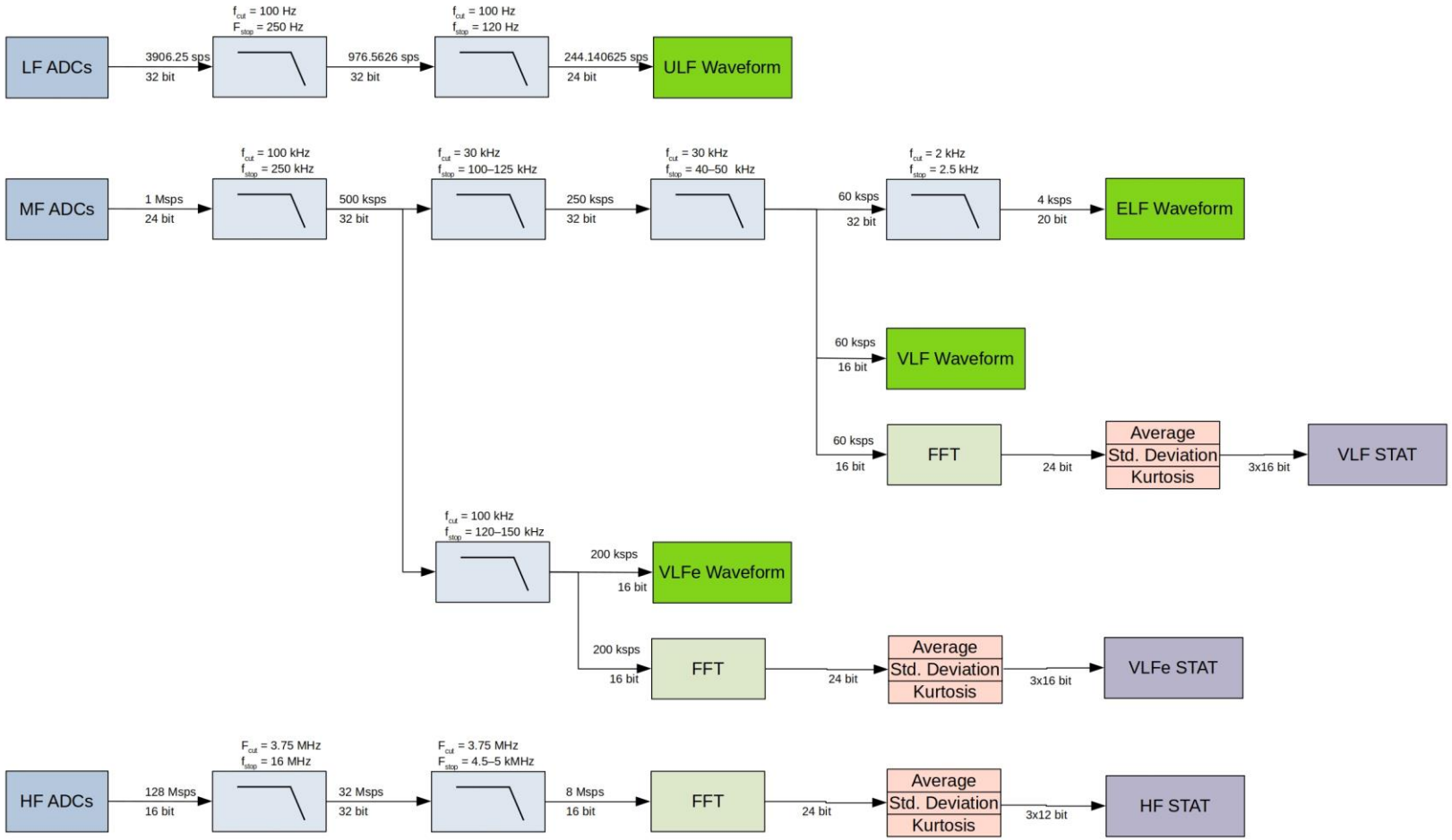

The digital filters are implemented by generating a coefficient file with Matlab and using the Xilinx Vivado FIR Compiler LogiCORE IP.

Statistical functions block

Data coming from the FFT block is used in a math block that calculates three statistical functions on these data stream.
If we define $x_i[j]$ as the j-th sample (with j ranging from 0 to 1023) of the i-th FFT sequence, and M=50 as the number of sequences we consider, then we define:

1. Average of M sequences: $\mu[j] = \frac{1}{M}\sum_{i=0}^{M-1} x_i[j]$
2. Standard deviation of M sequences: $\sigma[j] = \sqrt{\frac{1}{M}\sum_{i=0}^{M-1}(x_i[j] - \mu[j])^2}$
3. Kurtosis of M sequences: $k[j] = \frac{1}{\sigma^4[j]}\frac{1}{M}\sum_{i=0}^{M-1}(x_i[j] - \mu[j])^4$

This calculation is resource-intensive because the average can only be determined once 50 sequences have been received.

Not feasible on an FPGA with limited resources

Why do we calculate statistical functions instead of sending the data?

- Averaging FFT over 50 sequences allows a substantial payload reduction (mission constraint), at the cost of losing precision in signal detection.
- To re-gain information on sampling population distribution, we add Standard Deviation and Kurtosis.
- Kurtosis represents a measure of anomaly presence: deviation from the normal distribution.
- Combined analysis of Standard Deviation and Kurtosis allow the detection of a certain signal over the background.

Statistical functions implementation

The hardware architecture employs **basic polynomial properties,** allowing us to express the **standard deviation** using the provided definition of $\mu[j]$ as follows:

$$\sigma^2[j] = \left(\frac{1}{M} \sum_{i=0}^{M-1} (x_i[j])^2 \right) - \mu^2[j]$$

and for the **kurtosis:**

$$k[j] = \frac{1}{\sigma^4[j]} \left(\frac{1}{M} \sum_{i=0}^{M-1} (x_i[j])^4 - \frac{4\mu[j]}{M} \sum_{i=0}^{M-1} (x_i[j])^3 + \frac{6\mu^2[j]}{M} \sum_{i=0}^{M-1} (x_i[j])^2 - 3\mu^4[j] \right)$$

This results in a **parallel implementation** for calculating the sum of the first four powers of $x_i[j]$.
The hardware block responsible for summation utilizes a BRAM with 1024 memory locations to temporarily store intermediate data and sums the incoming data values according to the order of the FFT bin index.
After processing 50 sequences, these values are averaged by dividing them by $M = 50$ before being passed on to the subsequent pipeline stages.
The final 8 stages of computation involve multiplications between terms and constants, followed by the calculation of square roots, addition and subtraction operations, and division by $\sigma^2[j]$ to complete the computation.

The hardware is capable of processing one data input per clock cycle. Registration stages are intentionally incorporated to synchronize data with the j-th sample.

Statistical functions implementation

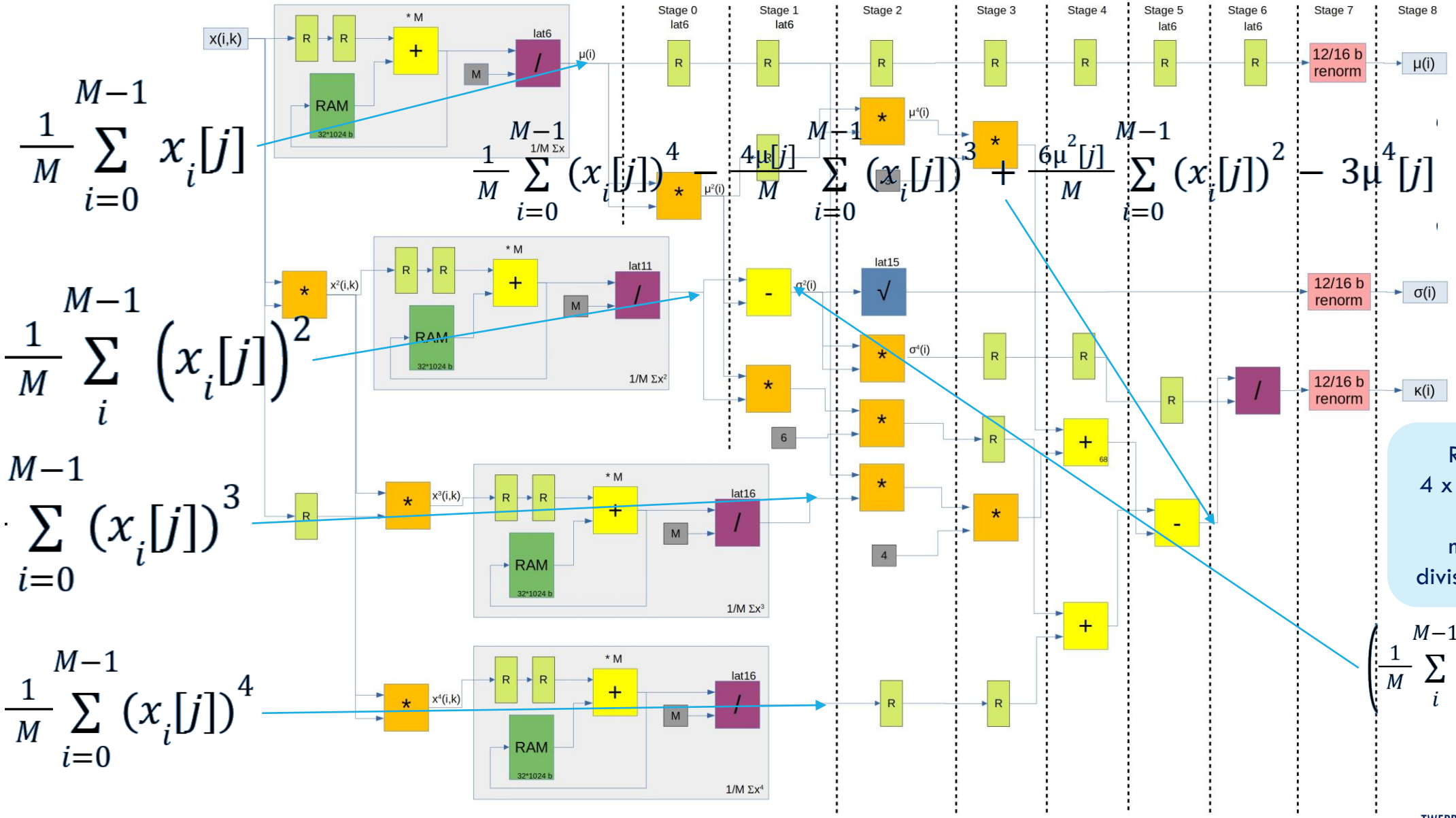

$$\frac{1}{M}\sum_{i=0}^{M-1} x_i[j]$$

$$\frac{1}{M}\sum_{i=0}^{M-1} \left(x_i[j]\right)^2$$

$$\sum_{i=0}^{M-1} \left(x_i[j]\right)^3$$

$$\frac{1}{M}\sum_{i=0}^{M-1} \left(x_i[j]\right)^4$$

$$\frac{1}{M}\sum_{i=0}^{M-1} \left(x_i[j]\right)^4 - \frac{4\mu[j]}{M}\sum_{i=0}^{M-1} \left(x_i[j]\right)^3 + \frac{6\mu^2[j]}{M}\sum_{i=0}^{M-1} \left(x_i[j]\right)^2 - 3\mu^4[j]$$

$$\left(\frac{1}{M}\sum_{i}^{M-1} \left(x_i[j]\right)^2\right) - \mu^2[j]$$

Resource usage:
4 x 1024 Block RAM;
8 add/sub; 9 multiplication; 5 division; 1 square root

Integer vs custom float

Due to payload constraints, the integer-based architecture lacked the required precision. Therefore, a **custom floating-point computation architecture** was developed to achieve better and adequate precision for the experiment.

Several implementation are compared:

- 12-bit (for HF) and 16-bit (VLF and VLFe).
- Integer fixed point arithmetic with output format ranging from 9.3 to 7.9
- 32-bit floating point arithmetic with output format casted to 12/16-bit integer fixed point.
- 32-bit floating point arithmetic with output format casted to **custom** 12/16-bit floating point.

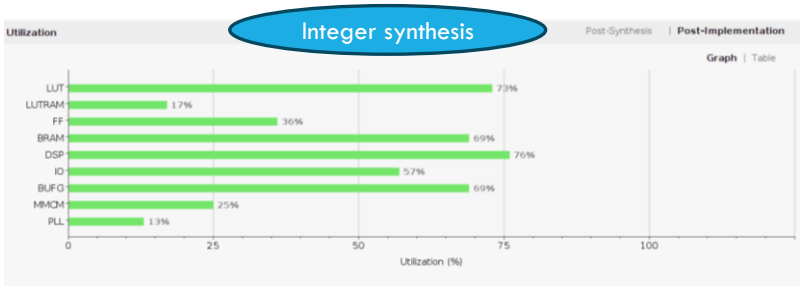

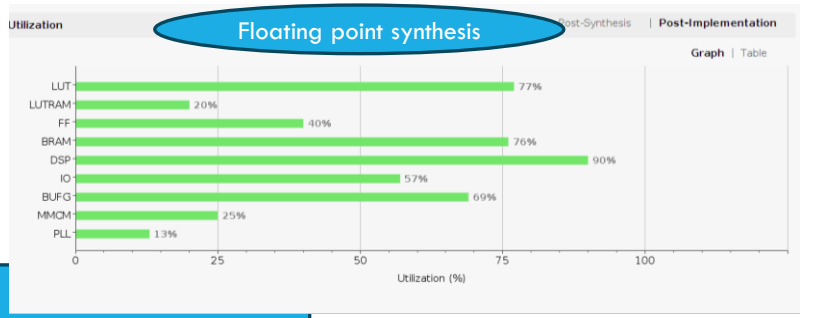

16-bit fp definition:

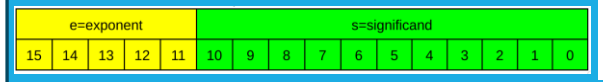

$$num_{16\,bit} = 2^{e-15}\left(1 + \frac{s}{2^{11}}\right)$$

12-bit fp definition:

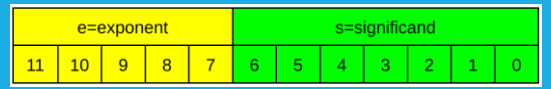

$$num_{12\,bit} = 2^{e-15}\left(1 + \frac{s}{2^{7}}\right)$$

Precision error definition:

$$10log_{10}\left|\frac{sw - hw}{sw}\right|$$

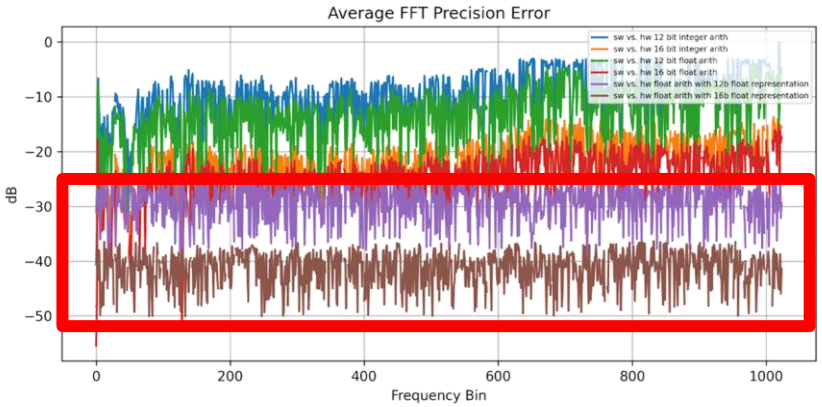

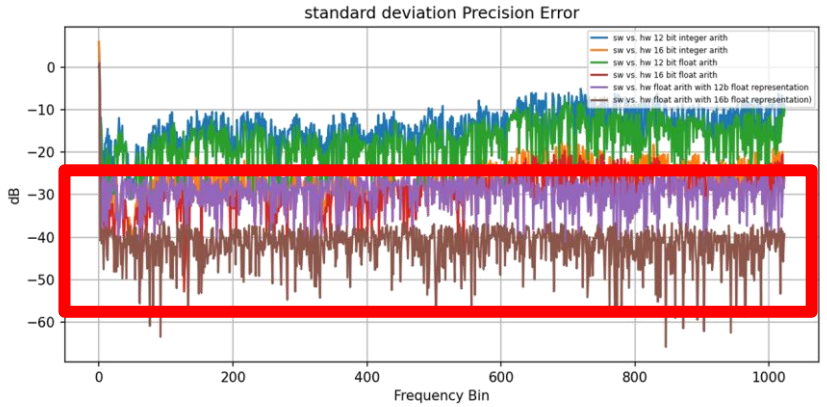

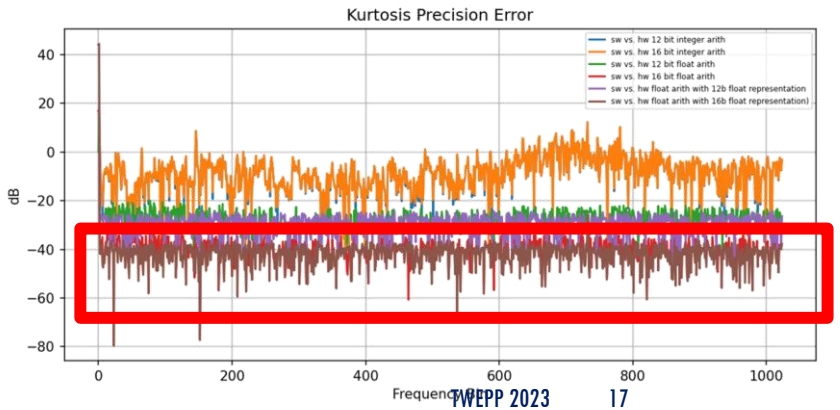

EFD System Verification

Characterizing the instrument on ground

from its prototype stage up to the flight model (FM)

CF variability:

between channels at different amplitudes and frequencies of the applied signal

Verification tests

In Climatic Chamber

Matrix of conversion factors (CF) - accurate calibration of the system - between digitized signals and voltage signals applied to the Electric Field Probes (EFP)

- Electronic transfer function
- Functionality
- Performances
- Ground calibration.

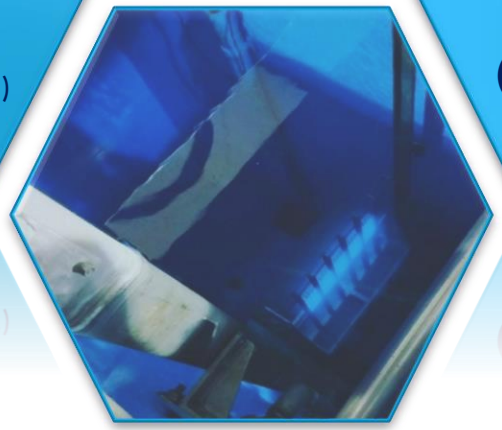

Qualification tests with **gamma irradiation**

(only on analog section)

Measurements in **ionospheric plasma,** a realistic environment for a satellite in LEO orbit, through a **Plasma Chamber.**

EFD System Verification

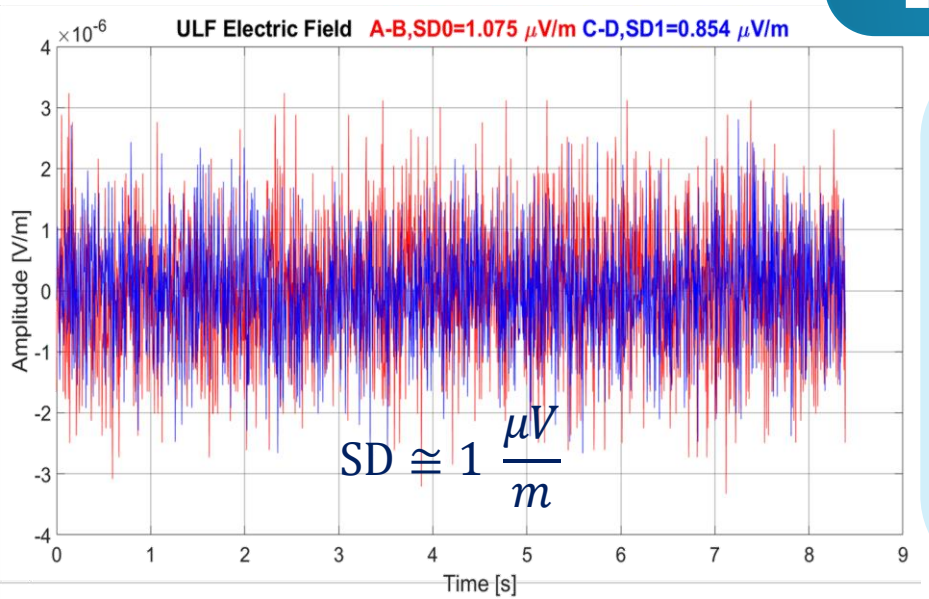

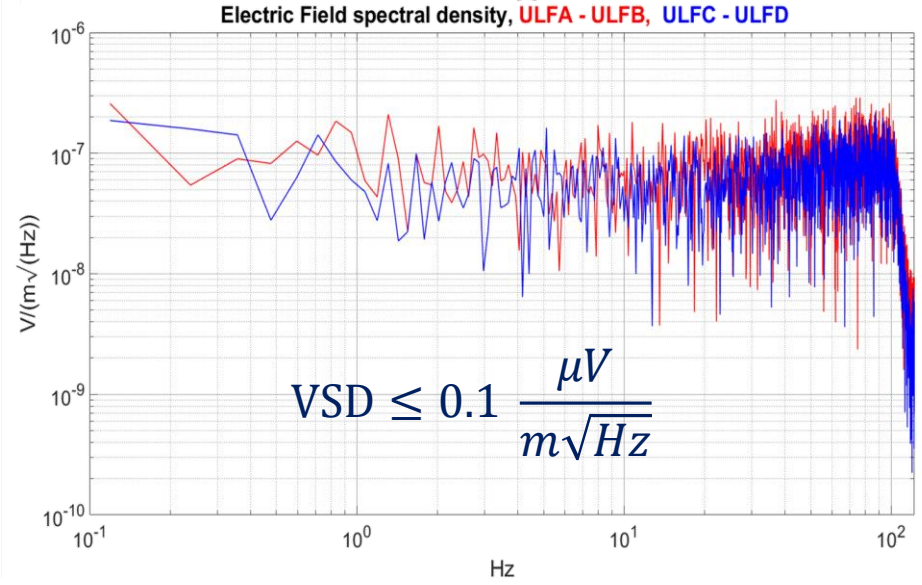

$$\mathrm{DR_{ULF}} \cong 120\ dB$$

EFD-02 noise analysis was conducted, both in the time and in the frequency domain.

The results demonstrate that all the specifications are met, in terms of signal to noise ratio and dynamic range.

Tests were satisfactory and reflect the expected requirements

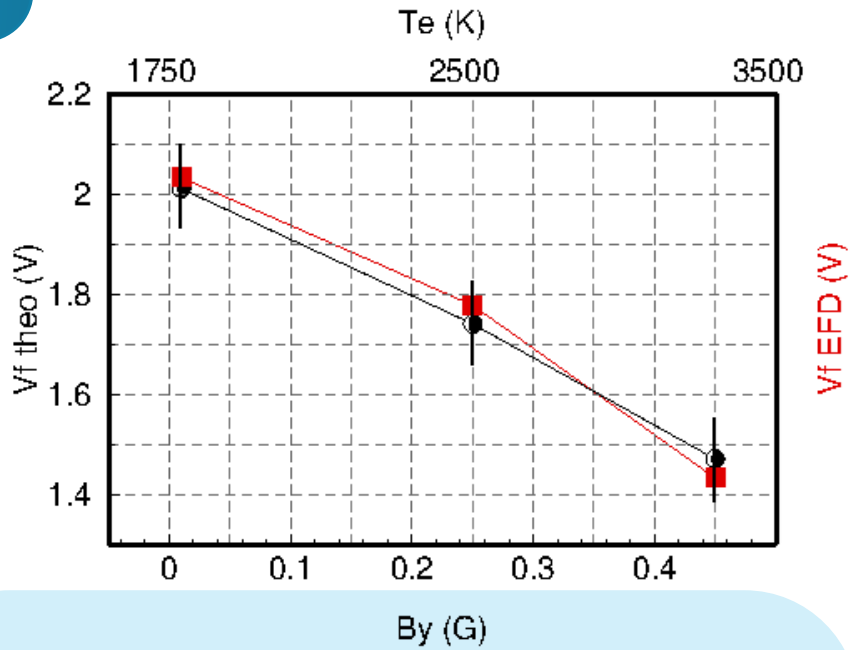

Tests with a **plasma source** have been particularly important because they have assessed that **EFD-02 make possible an** accurate evaluation of particle collection on the probe's surface, such as those induced by variations in Earth's magnetic field, By, parallel to SC direction.

The theoretical V_f values were computed by using plasma density and electron temperature obtained by Langmuir probes. **The OML expected results (black) together with the measured ones (red) are shown in figure.**

Conclusions

The focus of this work encompasses **not only the implementation** of Real-time Signal Processing and Data Acquisition for EFD-02 but also **the optimization of hardware resources** utilization on the digital board, all within the context of the stringent constraints posed by the impending space mission (scheduled to fly aboard the satellite of the CSES-02 mission in 2024).

Main topics discussed in this talk:

- Scientific studies that motivated CSES mission, presenting the most accredited theories and models that link seismic events and precursor from space.
- The cutting-edge characteristics of EFD-02 in measuring with great precision the electric field and its novelties.
- Description of the DPU and the implemented architecture for obtaining filters for various bands and performing FFT calculations.
- The significant optimization of the implementation of statistical functions to reduce computational resources used in calculations and the analysis conducted to select the optimal data representation.
- Finally, a series of tests were presented to verify the robustness of the EFD-02 system and ensure that it met all expected characteristics.

Current Mission Status

- EFD-02 QM has been successfully tested on board the CSES-02 satellite.
- EFD-02 FM will be shipped to China in the second half of October 2023.
- By mid-November 2023, EFD-02 FM will be installed on board the CSES-02 satellite for the final calibration.

This activity is essential as preparation for the subsequent commissioning phase, which will take place once the satellite is in orbit.

Thank you

Backup

Digital Processing Unit (DPU)

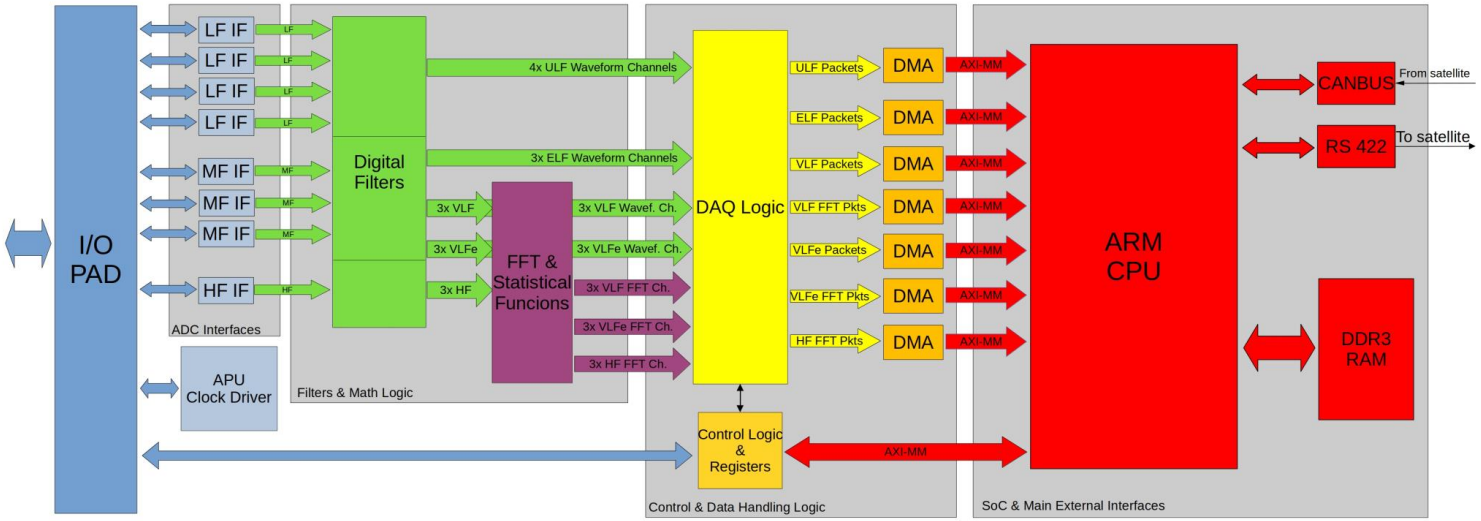

1.IO PAD: This block handles signal conditioning for interfaces toward the APU board. It manages input and output buffers, high-speed clock management, and DDR HF signal handling.

2.ADC Interfaces:

1. **Low Frequency ADCs (LF)**: This interface deals with configuration and data handling from four analog LF ADCs. It configures ADCs at power-on or system reset, serializes data, and operates at a 32-bit width and 3906.25 samples per second.
2. **Medium Frequency ADCs (MF)**: This interface handles configuration and data from three analog MF ADCs, with a 24-bit width and 1 Mega-sample per second sampling rate.
3. **High Frequency ADC (HF)**: This interface manages data from the single HF ADC, which multiplexes three channels on the APU board. It operates at a 128 MHz clock.

3.APU Clock Driver: This block programs the APU board clock driver at boot or system reset using a dedicated SPI channel.

4.Filters & Math Logic: This functional block processes digitized data from ADCs by applying digital filters to generate various bands, calculating FFT on selected bands, and performing statistical functions on spectral data.

5.Digital Filters:

1. **ULF Band**: Derived from LF signals with cascading low-pass filters.
2. **ELF, VLF, and VLFe Bands**: Derived from MF signals with cascading low-pass filters.
3. **HF Band**: Derived from HF signals with cascading low-pass filters.

6.FFT: Performs FFT on VLF, VLFe, and HF waveforms with specific characteristics.

7.Statistical Functions: Calculates average, standard deviation, and kurtosis of data from FFT, with both fixed-point and floating-point implementations.

8.Control and Data Handling Logic: Manages data encoding for DMA operations to the ARM CPU DDR3 memory, communication with the APU board, and control via AXI memory-mapped registers.

9.Registers: Provides a map of memory-mapped registers used to configure and read status from various parts of the system.

10.Data Acquisition Logic: Organizes data acquisition into seven DAQ modules for each band, performing data scheduling, packetization, and multiplexing.

Plasma Chamber measurements

The theoretical V_f values were computed by using plasma density and electron temperature obtained by Langmuir probes. **The OML expected results (black) together with the measured ones (red) are shown in figure.**

The observed V_f decrease for increasing By (parallel to Plasma Chamber) **is an expected behavior** caused by the smaller electron gyro-radius and the relative forced motion of the electrons around the probe surface which, in turn, reduces the electron saturation current.

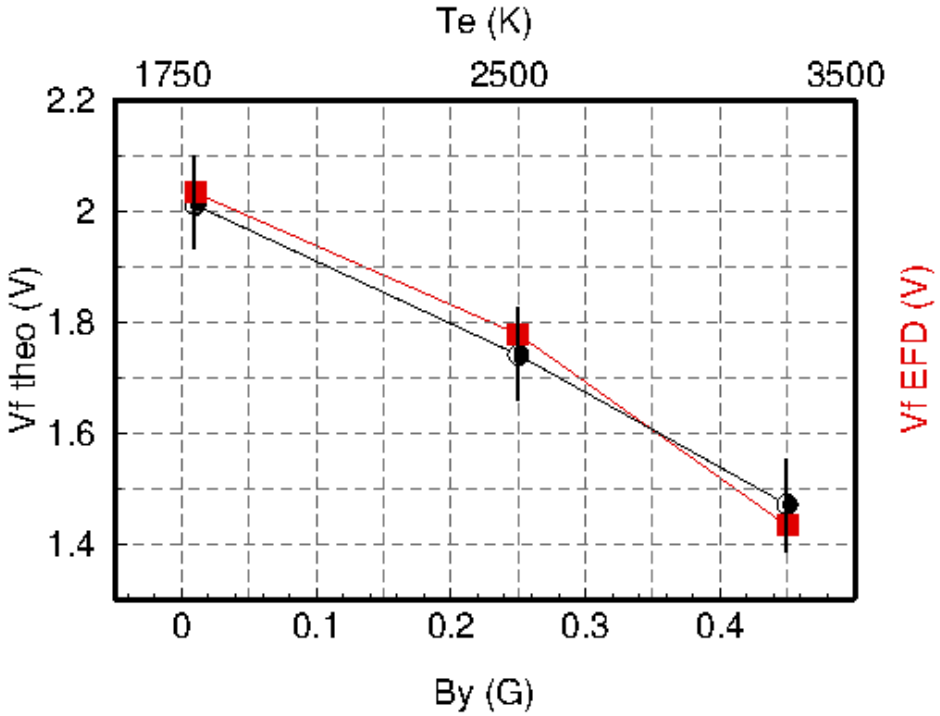

In addition, an **increased electron temperature** (Te) **is observed as expected** from the reduced slope of the characteristic curve of the sensors.

Moreover, **the V_f reduction** is also coherent with the rule of thumb establishing that V_f is a few $k_B T$ lower than the plasma potential V_{pl} ([79], and reference therein). Then, when V_{pl} is constant, **V_f decreases for increasing Te** (as shown in the top horizontal axis in figure).

Gamma irradiation tests

I qualified the APU under gamma irradiation, to verify its resistance to spatial radiation in LEO (Low Earth Orbit) **from the point of view of the effects caused by the Total Ionizing Dose** (TID). The radiation resistance of the APU EM prototype was tested by gamma irradiation at the Calliope Gamma Irradiation Facility of ENEA Casaccia in June 2021. (Source 60Co, two photons of 1.17 and 1.33 MeV energy emitted in coincidence)

In studying the aging of the APU board and verifying system-level functionalities, **keeping the system under test powered and active for the entire throughout of the measurements.**

Although probably present, SEE-type events were not kept under control and only an overall dose check was performed on the whole system, with no test on individual electronic components.

I helped in the logistic organization of the instrumentation necessary for tests. I helped in setting up the test set-up and in the assembly of the **protective screen** of the part of the apparatus to be protected from radiation (bricks and PB slabs). I personally conducted every day of testing, who aimed to verify:

- **Electric functionality:** power supply and controls.
- **Performance:** offset of the channels; transfer function; dynamic range and linearity; intrinsic noise.

Gamma irradiation tests

The **APU was placed** within the irradiated area at a **specific location** where the **total dose** received by the board (using multiple dosimetric methods) was of **10 krad,** with total daily dose of about 1 krad (~ 42 rad/h); the radiation non-uniformity on the DUT was <20%. The APU was the only board exposed, as to ensure that any failure due to radiation was attributable to the APU alone.

[Samwel, Susan & Hady, A. A. & Mikhail, J.S. & Ibrahim, Makram & Hanna, Yousry. (2008)]

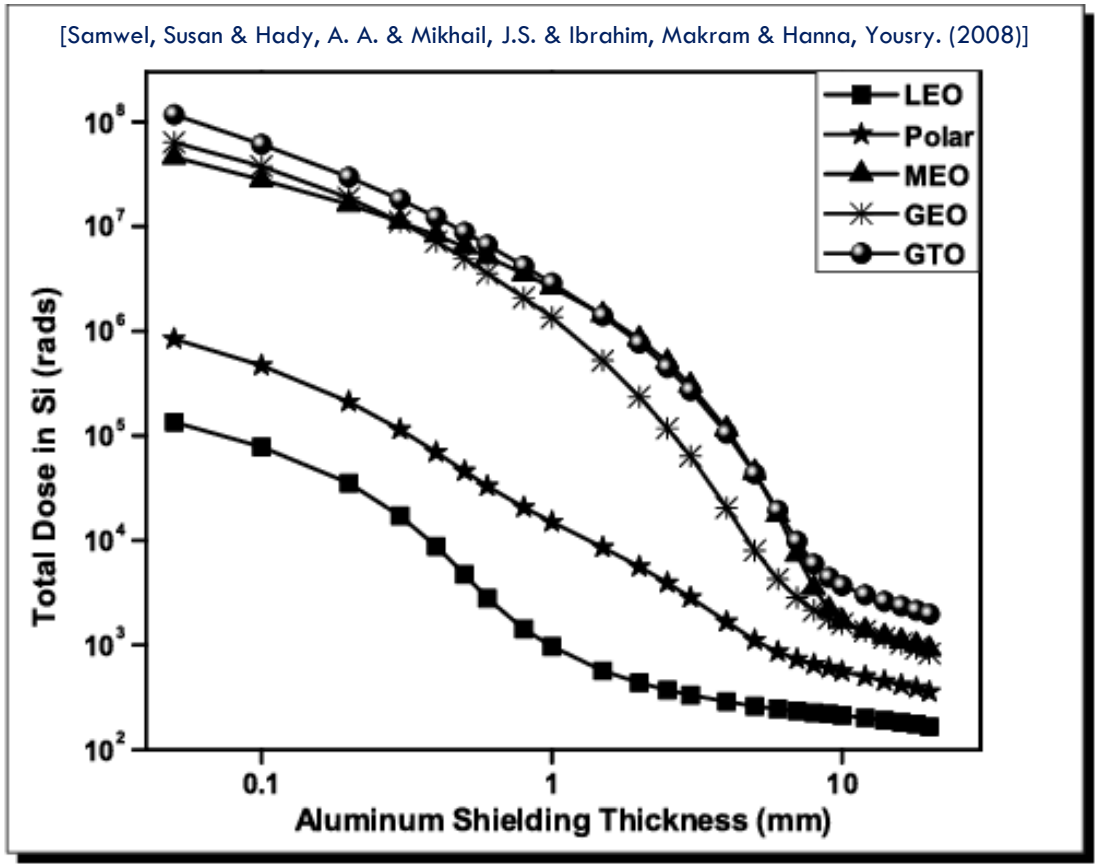

A spacecraft in an orbit LEO experiences the lowest doses.

It is also worth noting that the **test was very conservative** with respect to the radiation environment that the satellite will encounter in its trajectory.

Considering the CSES-02 mission profile and the position of APU board within the satellite, **the expected TID for the board in 6 years of mission is less than 0.5 krad**

General overview: early observations, previous missions and models

SEISMIC-RELATED PHENOMENA

- **Early Observations**
  - Missions non–dedicated to seismic investigation or reanalysing data from other missions: Intercosmos 19, Aureol 3, GEOS 1 and 2, Intermoscos-Bulgaria 1300, COSMOS-1809
- **The Radon coupling mechanism**
  - Due to radon exhalation from the soil, local fair-weather conductivity could increase up to 50%, whereas the electric field could decrease by 30% [17].
- **Thermal Anomalies**
  - Pre-seismic processes like release of radon and optically active gases (including carbon dioxide and methane) whose concentration could influence the thermal radiation emitted from the ground [18].
  - Several different parameters such as atmospheric temperature (at various altitudes), Brightness Temperature (BT), Surface Latent Heat Flux (SLHF), Outgoing Longwave Radiation (OLR)
- **Ionospheric Disturbances**
- **Acoustic Gravity Waves**
  - Anomalous fluctuation of the OLR satellite data (that can be related to thermal anomalies)
  - The occurrence of AGW of period of about 1 h.
  - Ground based detection of VLF disturbances.
- **Electromagnetic Field Measurements**
  - ICE on board the DEMETER: measured electric field anomalies (detected a few days before the earthquake was: from about 3 mV/km up to 100 mV/km on ground while about 3–5 mV/m at frequencies <0.5 Hz (relative variation >4%) for space data [21].
- **Particle Precipitation from Van Allen Belts**
  - Stable motion of high-energy trapped and quasi-trapped Van Allen particles can be perturbed also by seismo-associated EM emissions
- **Remote Sensing and Multi-Parametric Approach**
  - Possibility to monitor multiple parameters for precursor signatures in the simultaneous variation of several physical variables.
  - Survey large areas that could be affected by the earthquake preparation process but cannot be monitored with the network of scattered ground stations.

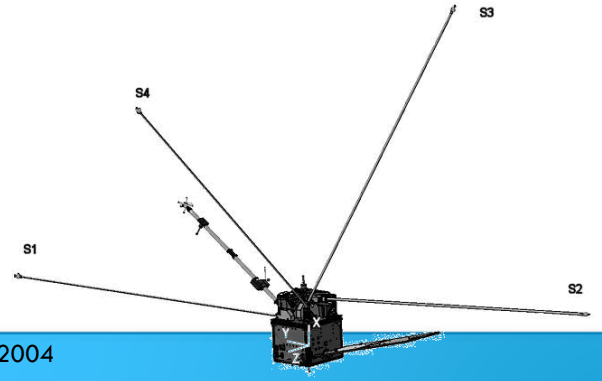

June 29, 2004

DEMETER SATELLITE OBSERVATIONS

- **Variability of electromagnetic precursors.**
- **Relation information between ground and space.**
- **Correlation between earthquake magnitude, depth, and amplitude of possible precursors.**
- **Extent of the spatial scale of the precursors.**
- **Temporal advance and clustering of anomalous observations.**

Sensor immersed in Plasma

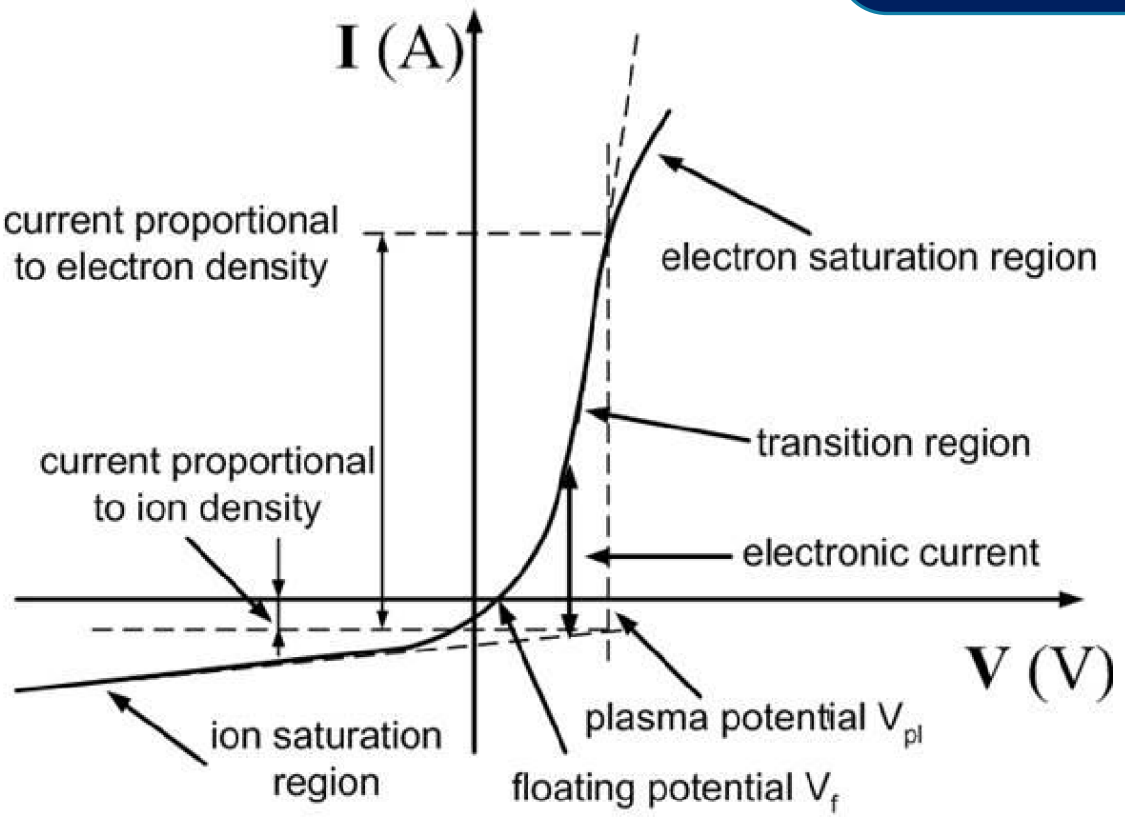

Characteristic of a conducting electrode in a plasma [68].

The probes of the EFD behave essentially as floating electrodes immersed within the ionospheric plasma. A conducting probe in contact with a plasma attains a potential (denoted as floating potential) which can be theoretically estimated by imposing that the net current collected by the probe surface is equal to zero.

In the case of the EFD probes, four contributions are relevant:

I. Electron collection.

II. Ion collection.

III. Photoelectron emission.

IV. Current injected to the probe (bias current source).

The floating potential condition can be expressed as:

$$\sum_{k=1,2,3,4} I_k = 0$$

The dynamical resistance R_{pl} at a point along the current-voltage curve is defined as the reciprocal of the derivative of the current with respect to the potential, according to:

$$R_{pl}^{-1} = \frac{dI_{tot}}{dV} \Big|_{V=V_0}$$

where V_0 represents the potential value at which the dynamical resistance is determined.

The contact resistance exhibits its minimum close to the plasma potential point (V_{pl}).

ULF – DC linearity

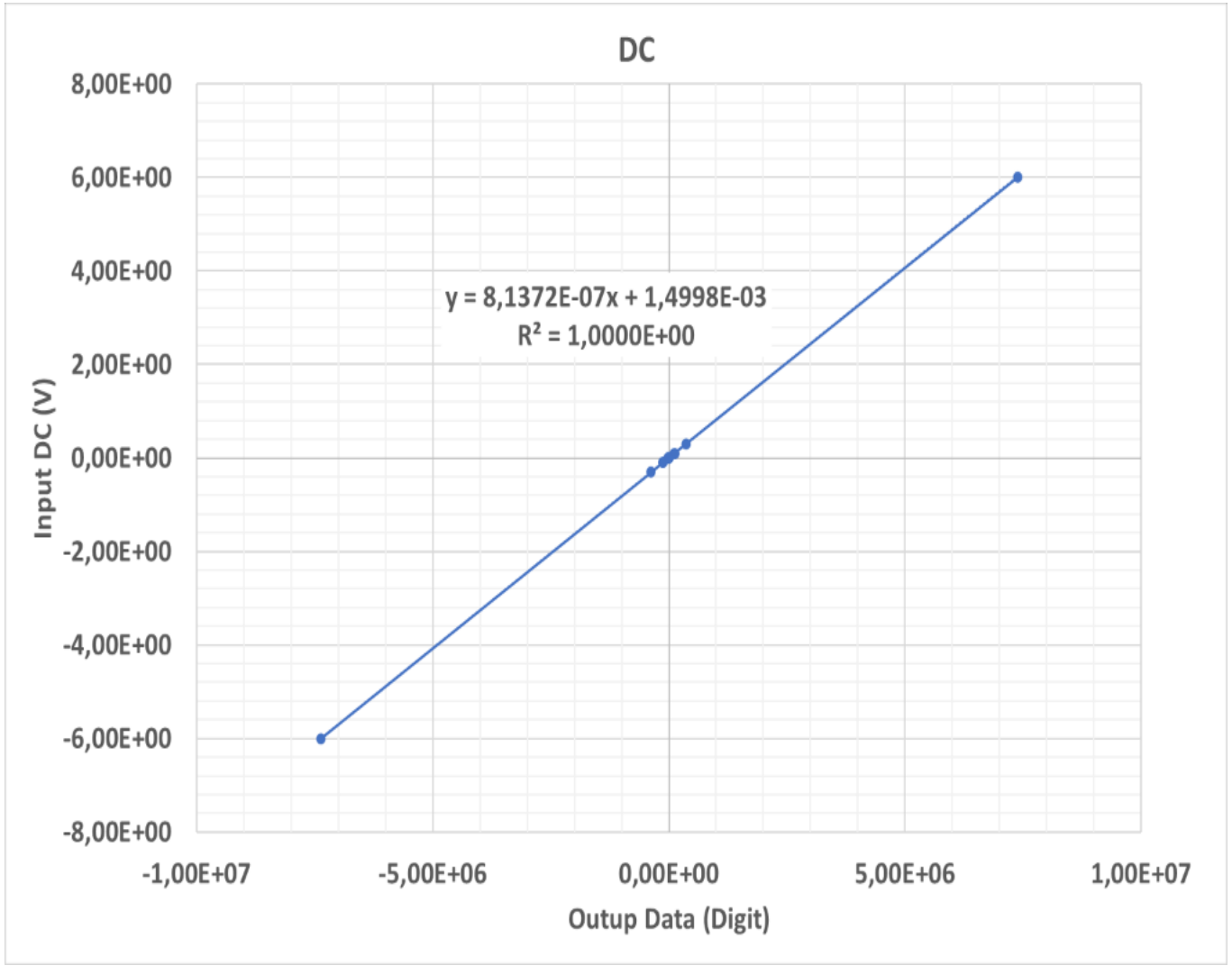

Shows the input in the **entire DC dynamic range** versus data.

The slope coefficient of the trend line represents the **best conversion factor value for amplitude changes,** excluding those with the smallest value of the input signal where the correspondent measurements of input signal are not considered sufficiently accurate for the calibration.

It is noteworthy that the linear trend fits perfectly with the experimental data.

Electric Field Probe (EFP)

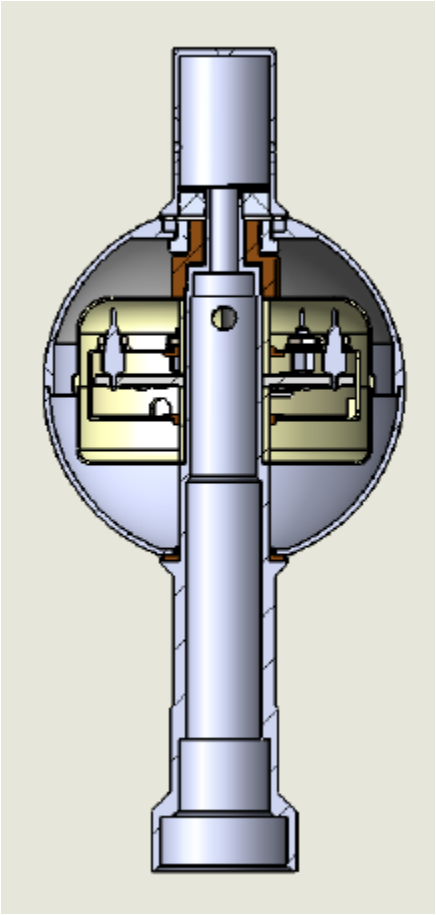

The EFP consists of a **spherical sensor located at the tip of a conductive boom.**
They are equipped with cylindrical conducting stubs bootstrapped at the electrode potential.
The architecture of the EFP sensor consists of **3 main blocks:**

- **Voltage follower** with low noise and high input impedance;
- **Bias Current injection circuit;**
- **Bootstrap circuit.**

a temperature sensor (PT-1000) allow the monitoring of the temperature inside the probe.

Inside **three concentric shells:**

- **Outermost** → serves as the measuring electrode.
- **Intermediate** → is bootstrapped to the output voltage of the preamplifier to minimize the capacitance to ground in parallel with the input preamplifier capacitance and to improve the frequency response.
- **Inner** → it is grounded and is a screen for the electronics.